Retrieval and Comparison of Forest Leaf Area Index Based on Remote Sensing Data from AVNIR-2, Landsat-5 TM, MODIS, and PALSAR Sensors

AUTHOR(S):

Chen, Wei; Yin, Hang; Moriya, Kazuyuki; Sakai, Tetsuro; Cao, Chunxiang

CITATION:

Chen, Wei ...[et al]. Retrieval and Comparison of Forest Leaf Area Index Based on Remote Sensing Data from AVNIR-2, Landsat-5 TM, MODIS, and PALSAR Sensors. ISPRS International Journal of Geo-Information 2017, 6(6): 179.

ISSUE DATE:

2017-06-21

URL:

http://hdl.handle.net/2433/233040

International Journal of Geo-Information

MDPI

Article

Retrieval and Comparison of Forest Leaf Area Index Based on Remote Sensing Data from AVNIR-2, Landsat-5 TM, MODIS, and PALSAR Sensors

Wei Chen [1,2,*,†], Hang Yin [1,†], Kazuyuki Moriya [2], Tetsuro Sakai [2] and Chunxiang Cao [1]

1 State Key Laboratory of Remote Sensing Science, Institute of Remote Sensing and Digital Earth, Chinese Academy of Sciences, Beijing 100101, China; yinhang@radi.ac.cn (H.Y.); caocx@radi.ac.cn (C.C.)
2 Biosphere Informatics Laboratory, Department of Social Informatics, Graduate School of Informatics, Kyoto University, Kyoto 606-8501, Japan; moriya@i.kyoto-u.ac.jp (K.M.); sakai@bre.soc.i.kyoto-u.ac.jp (T.S.)
* Correspondence: chenwei@radi.ac.cn; Tel./Fax: +86-10-6480-6228
† These authors contributed equally to this work.

Academic Editor: Wolfgang Kainz
Received: 24 March 2017; Accepted: 18 June 2017; Published: 21 June 2017

Abstract: Remote sensing data from multi-source optical and SAR (Synthetic Aperture Radar) sensors have been widely utilized to detect forest dynamics under a variety of conditions. Due to different temporal coverage, spatial resolution, and spectral characteristics, these sensors usually perform differently from one another. To conduct statistical modeling accuracies evaluation and comparison among several sensors, a linear statistical model was applied in this study for retrieval and comparative analysis based on remote-sensing indices from optical sensors of ALOS AVNIR-2 (Advanced Land Observing Satellite Advanced Visible and Near Infrared Radiometer type 2), Landsat-5 TM (Thematic Mapper), MODIS NBAR (Moderate Resolution Imaging Spectroradiometer Nadir BRDF-Adjusted Reflectance), and the SAR sensor of ALOS PALSAR (Advanced Land Observing Satellite Phased Array type L-band Synthetic Aperture Radar), respectively. This modeling used the forest leaf area index (LAI) as the field measured variable. During modeling, six optical vegetation indices were selected for evaluation and comparison between the three optical sensors, while simultaneously, two radar indices were calculated for the comparison between ALOS AVNIR-2 and PALSAR sensors. The gap between the spatial resolution of remote-sensing data and field plot size can account for the different accuracies found in this study. This study provides a reference for the selection of remote-sensing data types and spatial resolution in specific forest monitoring applications with different data acquisition costs and accuracy needs. Normally, at regional and national scales, remote sensing data with 30 m spatial resolution (e.g., Landsat) could provide significant results in the statistical modelling and retrieval of LAI while the MODIS cannot always meet the requirements.

Keywords: optical sensors; forest monitoring; leaf area index; vegetation index; PLS regression

1. Introduction

With significant developments in remote-sensing technology, a variety of satellites and sensors with different spatial, spectral, and temporal resolutions have been quickly developed. The launch of the Earth Resources Technology Satellite "ERTS-1" (i.e., Landsat-1) in the early 1970s is considered a milestone in the history of the development of satellite remote sensing. SEASAT, launched in 1978, was the first civilian satellite designed for remote sensing of the Earth's oceans with the first spaceborne synthetic aperture radar (SAR). In 1999, the first commercial satellite (IKONOS) collecting very high resolution imagery was launched. By far, more than 6000 satellites have been launched, over 60% of which serve military purposes. Those for civilian and scientific use mainly include the series of

Landsat, meteorological, ocean, geodetic, astronomical observation, and communications satellites. These satellites provide sufficient spatial and temporal coverage of high quality data at various scales. As a result, the potential of using remote-sensing techniques as a monitoring tool for forest ecosystems has been adequately recognized. Multi-source optical and radar data, including the widely recognized Landsat records [1], high spatial resolution Quickbird imagery [2], and time-series SPOT (Systeme Probatoire d'Observation de la Terre)-VEGETATION images [3] as well as L-band PALSAR data [4], have been widely utilized to monitor the forest status and its dynamics under various circumstances.

All remote sensing-based modeling can be traditionally classified into two major categories: physical and statistical. Physical models always follow the physical mechanisms of the remote-sensing systems and can be continuously improved by adding necessary knowledge. However, it is usually challenging to make clear the physical mechanisms of the interaction between surface objects and remote sensing signals, with the appropriate models also potentially being quite complex. On the other hand, statistical models are based on the correlation relationships between remotely sensed variables and land surface measurements. These types of models are usually site-limited. However, there are clear advantages in terms of the convenience for development, effectiveness for calculations, and fewer demands for input data [5].

In consideration of the limitations of specific physical models in data sources as well as input variable requirements, the statistical modeling approaches are suited for applications under different environmental conditions and imaging systems due to the above-mentioned advantages [6]. Thus, the simple linear regression model was chosen in this study for accuracy comparisons among different optical sensors with varied resolutions, as well as between optical and SAR sensors.

The leaf forms the main surface for matter and energy exchange between the vegetation canopy and the atmosphere. Leaf area index (LAI), which is the ratio of foliage area to ground area, is proposed as a key variable in the study of forest ecosystems and their development [7]. Chen and Black proposed using half of the total green leaf area in order to take into account the effective photosynthetic area in the case of non-flat leaves [8]. LAI can be used to characterize the canopy–atmosphere interface of an ecosystem and is related to precipitation, radiation extinction, canopy microclimate, atmospheric nutrient deposition, and interception as well as water, carbon, and energy exchanges with the atmosphere [9]. It plays a key role in the studies of various fields, including climate change, environment management [10], and vegetation surveys [11]. It can both be retrieved from remote-sensing data and measured using developed canopy analyzer devices [8]. In this study, it was selected as the field measured variable to correlate with remote sensing-based spectral reflectance or its transformations.

With regard to the spectral characteristics of green vegetation in specific bands, they reflect their own biophysical features and environmental impacts. Thus, the surface reflectance of some specific spectral bands can be used to establish regression models with biophysical parameters [5,6]. Nevertheless, considering the differences in the wavelength range and bandwidth among different optical sensors, direct comparisons using single-band reflectance are limited and spectral indices can be derived and applied to improve the accuracy. As demonstrated in many previous studies, vegetation index (VI), a combination of single band of remote sensing data, can be treated as a simple, effective, and experienced characterization of ground vegetation conditions [12]. Previous studies have proven that the VI usually shows a good correlation with a variety of physiological and ecological parameters and hence can be widely used to diagnose a range of biophysical vegetation parameters, including canopy structural parameters [13], LAI [14], fractional vegetation cover [15], and above-ground biomass (AGB) [16]. Consequently, the VI was chosen as the remote-sensing extracted variable to form those linear regression models.

There is remote-sensing data from a wide variety of optical and radar sensors which had been adopted for forest detection, monitoring, and management. For example, Arroyo et al. integrated LiDAR (Light Detection and Ranging) data and high spatial resolution satellite imagery (Quickbird-2) to estimate riparian biophysical parameters and land cover types in Queensland, Australia [17]. Andersen et al. utilized a combination of ground plots, LiDAR strip sampling, multispectral and

radar imagery, as well as classified land cover information to estimate forest biomass resources in interior Alaska [18]. Furthermore, MODIS (Moderate Resolution Imaging Spectroradiometer), ALOS PALSAR (Advanced Land Observing Satellite Phased Array type L-band Synthetic Aperture Radar) and Landsat TM (Thematic Mapper) data had been selected to estimate forest LAI [19], growing stock volume [20], and aboveground carbon storage [21], respectively. The optical images and SAR datasets were also used for the forest disturbance detection and recovery monitoring [22,23]. As shown, these data have considerably different temporal coverage, spatial resolution, and even imaging mechanisms, hence demonstrating quite different performances among the various sensors. In the actual forest monitoring and management, we usually do not need the remote sensing data with the highest spatial resolution. In some cases, data with 30 m spatial resolution can meet the requirements, thus data with a spatial resolution of 10 m or even 1 m are unnecessary. Furthermore, remote sensing data with higher spatial resolution usually have higher acquisition costs. Thus, considering this, the actual needs and accuracy requirements should be fully evaluated to seek the most appropriate remote sensing data.

To make the statistical modeling accuracies evaluation and comparison among various sensors more direct and targeted, in this case, linear regression modeling was conducted using field measured LAI values and remote-sensing indices. These indices were calculated from four sources of data: ALOS AVNIR-2, Landsat-5 TM, MODIS NBAR (Nadir BRDF-Adjusted Reflectance), and ALOS PALSAR. These data were acquired at relatively close dates in 2010. During the modeling, six diverse optical vegetation indices were selected for the evaluation and comparison among the three optical sensors with different spatial resolutions. Following this, two radar indices defined in a similar form of corresponding optical indices were determined for the comparison between AVNIR-2 and PALSAR sensors. Both single-variable-based and multiple-variable-based modeling were performed, with the results being verified by cross-validation and then compared.

2. Materials and Methods

2.1. Study Area

The Greater Hinggan Mountain area, which spans the northern part of Heilongjiang Province and the Inner Mongolia Autonomous Region of China, is the watershed area of the Mongolian Plateau in the west and the flat Songliao Plain in the east. Its geographic coordinates range between 50°11′–53°33′ N in latitude and 121°12′–127°00′ E in longitude (Figure 1). The region has a total length of over 1200 km, a width of 200–300 km and an average altitude of 573 m. It is an important climatic zone, having a typical continental cold–temperate monsoon climate with warm summers and cold winters. The average annual temperature of the whole mountain area is −2.8 °C, with an average annual precipitation of 746 mm [11].

The Greater Hinggan Mountain area is China's northernmost and largest state-owned modern forest area, with a total ground area of 8.46×10^6 ha and a forest-covered area of 6.46×10^6 ha. The forest coverage is around 76.40%, providing a total stand volume of up to 5.01×10^8 m^3, which accounts for around 7.8% of the total national stand volume of China. It is a mixed forest area dominated by coniferous species, such as Mongolian pine (*Pinus sylvestris*) and Larch (*Larix gmelini*), and broad-leaved species, such as Birch (*Betula platyphylla*) and Aspen (*Populus davidiana*).

2.2. Remote-Sensing Data

In order to investigate and compare the application accuracy of optical remote-sensing data, the multi-source optical images of ALOS AVNIR-2, Landsat TM, and MODIS were selected for the comparative study in consideration of their different technical characteristics, especially spatial resolution. As described in Table 1, ALOS AVNIR-2 provides 10 m spatial resolution images with a repeat cycle of 46 days, while Landsat-5 TM has a spatial resolution of 30 m and temporal revisit cycle of 16 days. The MODIS aboard the Terra and Aqua satellites, operating in tandem, view the entire Earth's surface every one to two days, acquiring data in 36 spectral bands with ground resolutions of

250/500/1000 m. As these optical sensors have different objectives and show their specific advantages in different fields, the retrieval of LAI formed the focus of a more targeted comparative study. The same simple inversion method of statistical regression modeling was selected for the retrieval. Regarding the statistical modeling accuracies evaluation and comparison between optical and SAR sensors, it seems challenging since they have totally different physical mechanisms and data characteristics. In order to minimize the needless effects of other uncontrollable factors, the optical sensor of AVNIR-2 and radar sensor of PALSAR aboard the same ALOS satellite were chosen for comparison. PALSAR is an active microwave sensor using the L-band frequency under three observation modes to achieve cloud-free and day-and-night land observations (Table 2). Considering the data temporal coverage in the study area, the year of 2010 was determined as the time window for the three types of sensors.

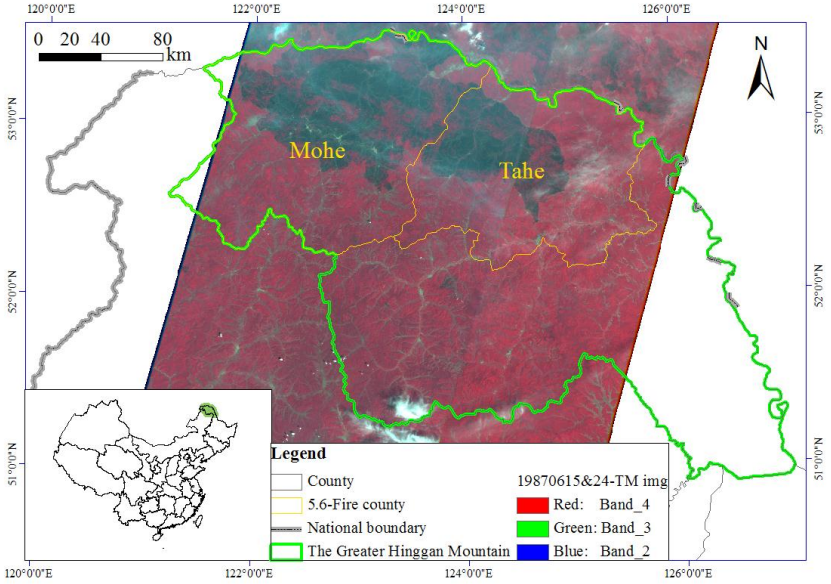

Figure 1. Location of the study area in the Greater Hinggan Mountains [11]. The background is the mosaic of two Landsat TM (Thematic Mapper) scenes acquired on 15 and 24 June 1987 (Red: band 4; Green: band 3; Blue: band 2).

Table 1. Radiometric characteristics of data from ALOS AVNIR-2 (Advanced Land Observing Satellite Advanced Visible and Near Infrared Radiometer type 2), Landsat-5 TM (Thematic Mapper), and MODIS NBAR (Moderate Resolution Imaging Spectroradiometer Nadir BRDF-Adjusted Reflectance) sensors.

Satellite	Sensor	Bands	Wavelength Range (μm)	Spatial Resolution (m)	Swath Width (km)	Repeat Cycle (days)
ALOS	AVNIR-2	1	0.42–0.50	10 (at Nadir)	70 (at Nadir)	46
		2	0.52–0.60			
		3	0.61–0.69			
		4	0.76–0.89			
Landsat-5	TM	1	0.45–0.52	30	185	16
		2	0.52–0.60			
		3	0.63–0.69			
		4	0.76–0.90			
		5	1.55–1.75			
		6	10.4–12.5	120		
		7	2.08–2.35	30		
Terra/Aqua	MODIS	1	0.620–0.670	250	2330 (cross track)	1-2
		2	0.841–0.876			
		3	0.459–0.479			
		4	0.545–0.565			
		5	1.230–1.250	500		
		6	1.628–1.652			
		7	2.105–2.155			

Table 2. Technical characteristics of the PALSAR (Phased Array type L-band Synthetic Aperture Radar) sensor.

Mode		Fine		ScanSAR	Polarimetric
		FBS	FBD		
Chirp bandwidth		28 MHz	14 MHz	14 MHz, 28 MHz	14 MHz
Polarization		HH or VV	HH+HV or VV+VH	HH or VV	HH+HV+VH+VV
Incident angle		8–60 deg.	8–60 deg.	18–43 deg.	8–30 deg.
Resolution	Range	7–44 m	14–88 m	100 m	24–89 m
	Azimuth	10 m (2 looks) 20 m (4 looks)		100 m	10 m (2 looks) 20 m (4 looks)
Swath width		40–70 km	40–70 km	250–350 km	20–65 km
Bit length		5 bits	5 bits	5 bits	3 or 5 bits
Data rate		240 Mbps	240 Mbps	120 or 240 Mbps	240 Mbps
Center frequency		1270 MHz (L-band)			
Radiometric accuracy		scene: 1 dB/orbit: 1.5 dB			

The ALOS AVNIR-2 image was acquired on 4 September 2010, and the Landsat-5 TM data was acquired on 2 September 2010. To maintain the consistency in acquisition date within a maximum limit, the MODIS products of Nadir BRDF-Adjusted Reflectance data (NBAR, MCD43A4) covering 29 August–13 September (Julian day of 241–256) were used. A superimposed map of the three scenes from AVNIR-2, Landsat-5 TM, and MODIS is shown in Figure 2. Considering the acquisition date of the AVNIR-2 image, the PALSAR data acquired on 13 August 2010 was used in this study. It has an incidence angle (at the scene center) of 38.701° as well as the dual-polarization of HH and HV. The same approach of linear regression modeling was adopted using the same collection of field measured LAI values. The AVNIR-2 and PALSAR images have the same spatial resolution of 10 m, which greatly facilitates effective comparison. A superimposed map of the two images from ALOS AVNIR-2 and PALSAR is shown in Figure 3.

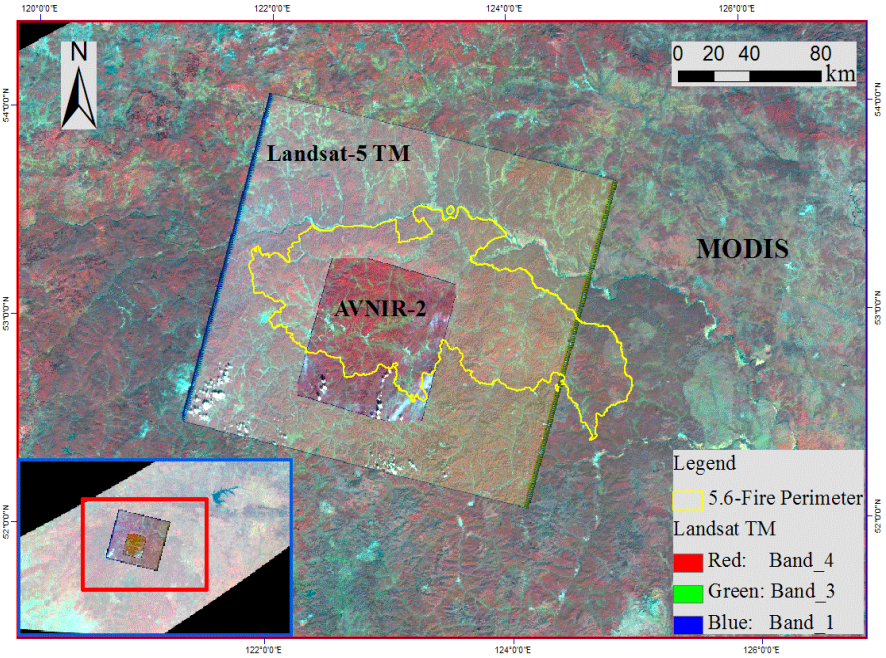

Figure 2. A superimposed map of three scenes from ALOS AVNIR-2, Landsat-5 TM, and MODIS (The red, green, and blue colors refer to the image color compositions).

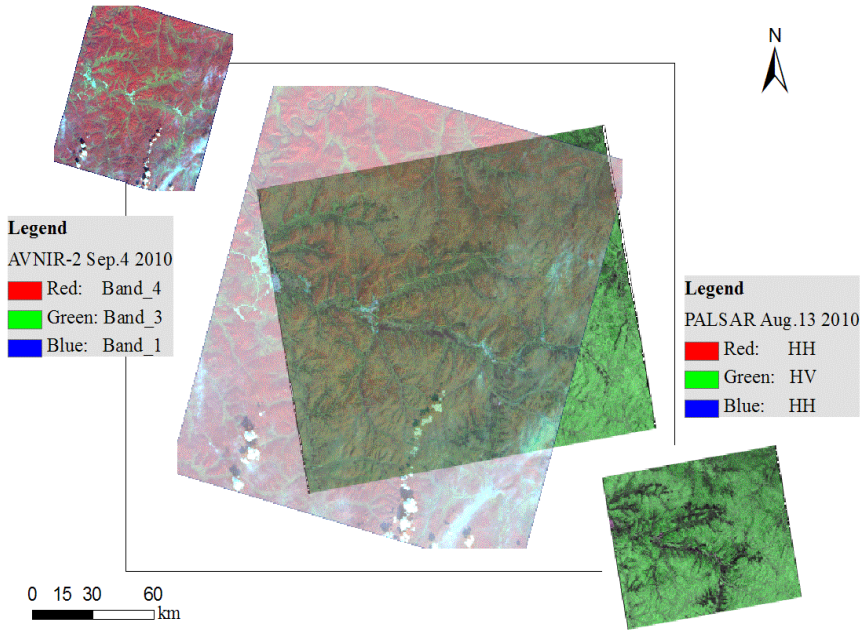

Figure 3. A superimposed map of two images from the optical sensor of AVNIR-2 and radar sensor of PALSAR aboard ALOS. For the overlap image in the middle, there is a transparency of 50% (The red, green, and blue colors refer to the image color compositions).

2.3. Field LAI Measurements

To collect the field data, a field forest survey was designed and conducted in July 2012 [11]. In this survey, a total of 18 plots located in the three forestry bureaus (Xilinji, Tuqiang and Amuer in Mohe, Heilongjiang, China) of the Greater Hinggan Mountain area with a size of 10 × 10 m were investigated and the locations of each plot were measured using a differential global positioning system (DGPS). Following this, a series of forest parameters (e.g., tree height, diameter at breast height, crown width, LAI) were measured. The LAI of each plot was measured using the LAI-2200 canopy analyzer with a height of just above the canopy (with the help of stepladder) under stable weather conditions. It makes the measured LAI the same as those near the crown of the tree (as measured by satellite) and thus available for the statistical modeling with remote-sensing indices.

In each plot of 10 × 10 m, LAI-2200 measurements were performed for five measuring points (red points in Figure 4) and an average value was calculated for the plot. The LAI-2200 device enables fast, non-destructive, and on-site computation of LAI from measurements made above the canopy, which are utilized to determine canopy light interception at five angles. These data are fit to a radiative transfer model to estimate LAI and some other parameters. This device measures up to a 360° azimuthal view for each zenith angle. It provides a large sample area for good spatial averaging. It can measure small plots and isolated plants. When measuring the plot values, the sampling regulations and measuring methods are the same for coniferous forest and broad-leaved forest.

Although there were two years between the acquisition dates of remote-sensing images and field data collection, the study can still be conducted as the main objective was focused on the comparison of the statistical modeling accuracies among the four sensors and the data from these sensors were acquired at approximately the same time.

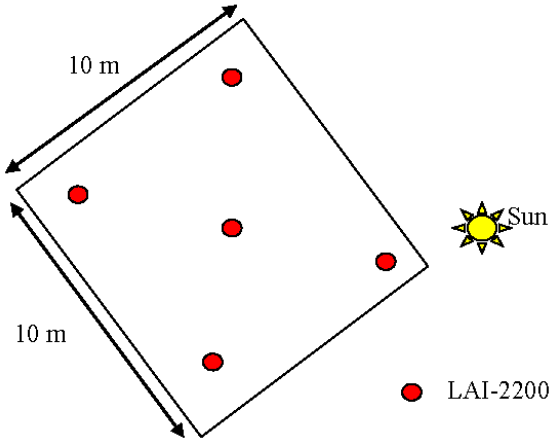

Figure 4. Sketch map of LAI measurements using LAI-2200.

2.4. Data Pre-Processing

The ALOS AVNIR-2 and Landsat-5 TM images were pre-processed by radiometric calibration, atmospheric correction, geometric correction, and orthorectification. After this, the surface reflectance of the study area was acquired. As the field sampling plots were located in the mountainous area where the terrain fluctuates greatly, terrain correction was applied using ASTER GDEM (Advanced Spaceborne Thermal Emission and Reflection Radiometer Global Digital Elevation Model) data. The MODIS NBAR data has already standardized reflectance to a nadir view, thus minimizing artifacts in the sample related to variable geometry. Additionally, the NBAR spectral bands are comparable to those of Landsat TM, as summarized in Table 1. The PALSAR data used is the level 1.1 data which corresponds to single look complex (SLC) products, provided in slant range geometry. It was pre-processed to back-scatter the intensity of (Sigma0: σ°) images through ALOS de-skewing, multi-look (one look in range direction and four looks in azimuth direction), speckle filter (median filter with window size of 3 × 3 pixels), as well as SARSim-Terrain correction (SRTM data; Root Mean Square threshold < 0.5 pixel) using the tools of NEST (Next ESA SAR Toolbox).

Since the ALOS AVNIR-2 and PALSAR imagery, Landsat-5 TM and MODIS NBAR data have completely different spatial resolutions of 10, 30, and 500 m, respectively, while the LAI data were acquired from field survey sampling plots with a size of 10 × 10 m, the images of Landsat-5 TM and MODIS NBAR were resampled to that of 10 m, making the spectral values extracted from optical images to be in the same spatial scale as the measured LAI values.

2.5. Multivariate Selection and Calculation

In this study, when building the relationships between optical vegetation indices (VIs) and field measured LAI, the impact of soil background and atmosphere was taken into account and thus, six indices were finally selected and statistically correlated to field measured LAI. These indices were the Ratio Vegetation Index (*RVI*) [24], Difference Vegetation Index (*DVI*) [25], Normalized Difference Vegetation Index (*NDVI*) [26], Soil-Adjusted Vegetation Index (*SAVI*) [27], Atmospherically Resistant Vegetation Index (*ARVI*) [28], and Enhanced Vegetation Index (*EVI*) [29], which were expressed as Equations (1)–(6), respectively

$$RVI = \rho_{NIR}/\rho_{Red} \quad (1)$$

$$DVI = \rho_{NIR} - \rho_{Red} \quad (2)$$

$$NDVI = (\rho_{NIR} - \rho_{Red})/(\rho_{NIR} + \rho_{Red}) \quad (3)$$

$$SAVI = (1 + L_1)\cdot(\rho_{NIR} - \rho_{Red})/(\rho_{NIR} + \rho_{Red} + L_1) \quad (4)$$

$$ARVI = (\rho_{NIR} - \rho_{RB})/(\rho_{NIR} + \rho_{RB}) \quad (5)$$

$$EVI = 2.5 \cdot (\rho_{NIR} - \rho_{Red})/(\rho_{NIR} + C_1 \cdot \rho_{Red} - C_2 \cdot \rho_{Blue} + L_2) \quad (6)$$

where ρ_{NIR},ρ_{Red}, and ρ_{Blue} denote the reflectance in the near-infrared, red and blue bands, respectively. Then $\rho_{RB} = \rho_{Red} - \gamma(\rho_{Blue} - \rho_{Red})$ and γ, which indicates that the radiation correction coefficient of the optical path is assumed to be the recommended value (by Kaufman) of 1. The parameter L_1 in Equation (4) indicates a soil adjusted coefficient, which is normally assumed to be 0.5 for most regions. In Equation (6), we set C_1 = 6.0, C_2 = 7.5 and L_2 = 1, which was used in the production of MODIS VI products.

Considering the derivation methodology and application fields of optical vegetation indices (e.g., *NDVI* and *EVI*), it was proposed that we should derive some similar indices from the radar backscattering coefficients. In a similar way to *RVI* and *NDVI*, two radar indices were available to be calculated, namely Radar Ratio Vegetation Index (*RRVI*) and Radar Normalized Difference Vegetation Index (*RNDVI*). They are defined by

$$RRVI = \sigma_{0HH}/\sigma_{0HV} \quad (7)$$

$$RNDVI = (\sigma_{0HV} - \sigma_{0HH})/(\sigma_{0HV} + \sigma_{0HH}) \quad (8)$$

where σ_{0HH} and σ_{0HV} indicate the backscattering coefficient in *HH* and *HV* polarization, respectively.

After calculating the six optical indices and two radar indices, the Pearson correlation analysis was performed. With those showing significant correlations, linear regression models were established and subsequent ANOVA (Analysis of Variance) was conducted (Table 3). It should be noted that the cross-validation was incorporated in the statistical modeling since the number of field survey plots was not sufficient for the independent verification.

Taking into account the accuracy and applicability of the model, the partial least squares (PLS) regression algorithm was selected. PLS regression is a statistical model, which tries to find the multidimensional direction in the space of predictors that explains the maximum multidimensional variance direction in the variable space of observations [30]. The principal component analysis (PCA) was combined in the PLS regression to enable the smallest necessary number of orthogonal components.

3. Results

3.1. Univariate Modeling Using Optical VIs

3.1.1. ALOS AVNIR-2 Data

The modeling results based on AVNIR-2 data are shown in Table 3(a) and Figure 5. As expressed in the table, the correlation coefficient (R > 0.7) and determination coefficient (R^2 > 0.5) were both quite high and the Standard Error of the Estimate (SEE) was particularly small. The significant probability (Sig. < 0.01) indicated the accuracy and applicability of these models. Among the six VIs, *RVI* performed best with the highest R^2 (0.798) and R (0.893), followed by *ARVI* (R^2 = 0.718) and *NDVI* (R^2 = 0.652). The regression model based on *DVI* showed the lowest correlation.

Table 3. The model summary and ANOVA (Analysis of Variance) of single-VI-based models. The indices were derived from (a) ALOS AVNIR-2; (b) Landsat-5 TM; (c) MODIS NBAR and (d) ALOS PALSAR data.

Independent Variables [a]	R	R^2	SEE [b]	F Statistics	Sig.
(a) ALOS AVNIR-2					
RVI	0.893	0.798	0.349	63.318	0.000 **
DVI	0.720	0.517	0.539	17.186	0.001 **
NDVI	0.808	0.652	0.458	29.987	0.000 **
SAVI	0.766	0.586	0.499	22.733	0.000 **
ARVI	0.848	0.718	0.412	40.853	0.000 **
EVI	0.773	0.596	0.493	23.685	0.000 **
(b) Landsat-5 TM					
RVI	0.823	0.677	0.441	33.585	0.000 **
DVI	0.625	0.391	0.606	10.279	0.006 **
NDVI	0.750	0.562	0.513	20.567	0.000 **
SAVI	0.693	0.480	0.560	14.783	0.001 **
ARVI	0.756	0.570	0.509	21.281	0.000 **
EVI	0.702	0.493	0.553	15.538	0.001 **
(c) MODIS NBAR					
RVI	0.687	0.471	0.518	8.920	0.014 *
DVI	0.578	0.334	0.582	5.019	0.049 *
NDVI	0.664	0.440	0.533	7.879	0.019 *
SAVI	0.591	0.349	0.575	5.373	0.043 *
ARVI	0.668	0.446	0.531	8.051	0.018 *
EVI	0.644	0.415	0.545	7.094	0.024 *
(d) ALOS PALSAR					
RRVI	0.834	0.695	0.429	36.465	0.000 **
RNDVI	0.833	0.694	0.429	36.380	0.000 **

[a] Independent variables include constant; Dependent variable is measured LAI; [b] SEE: Standard Error of the Estimate; * Significant correlation ($0.01 < \text{Sig.} \leq 0.05$); ** Extremely significant correlation ($\text{Sig.} \leq 0.01$).

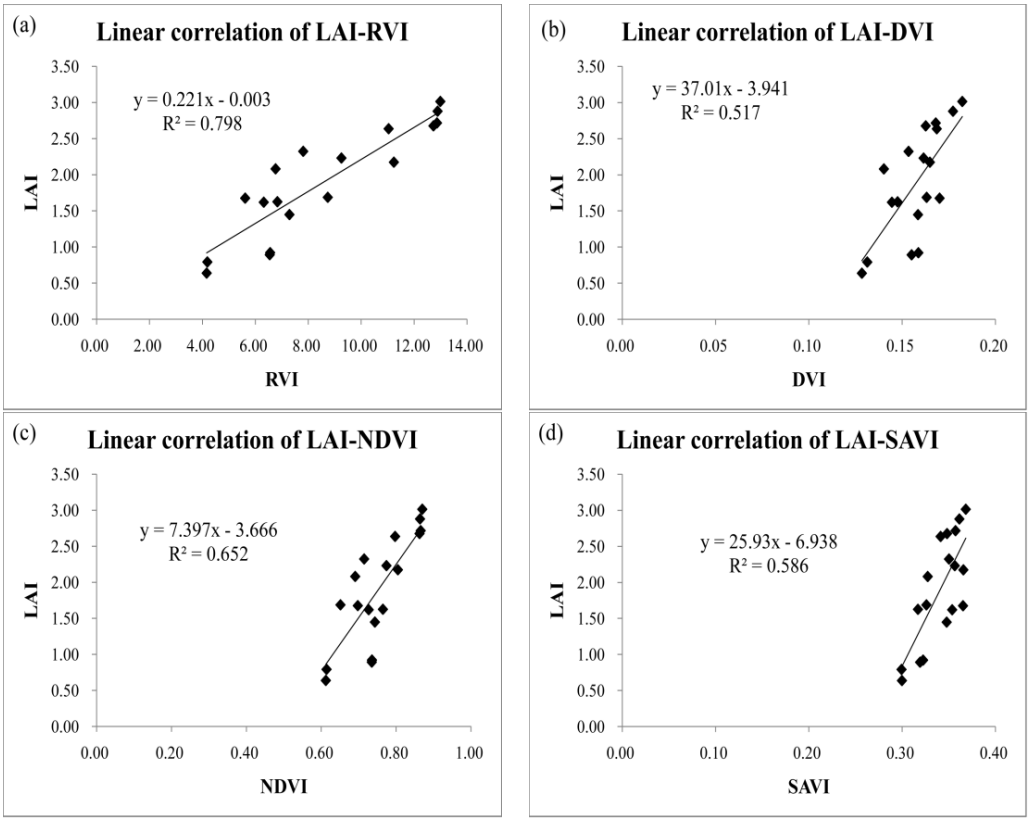

Figure 5. *Cont.*

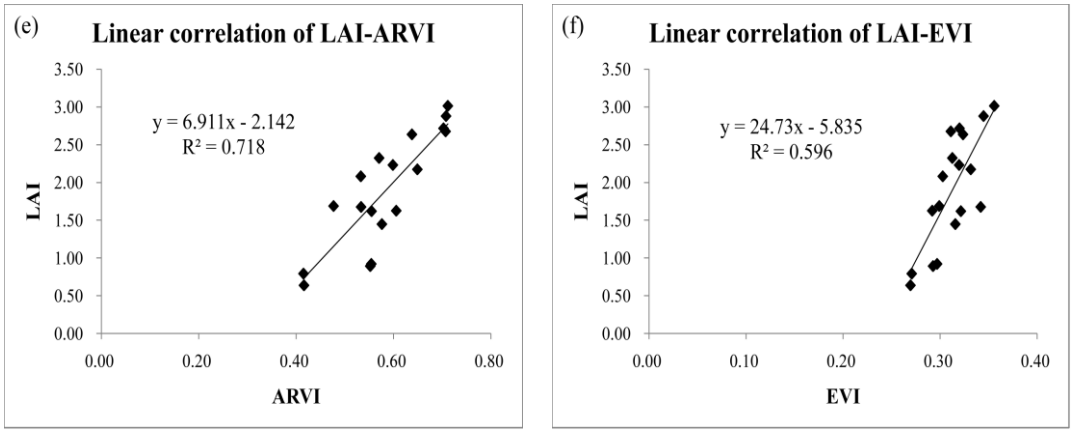

Figure 5. The linear regression models based on LAI and ALOS AVNIR-2-derived vegetation indices: (**a**) RVI (Ratio Vegetation Index); (**b**) DVI (Difference Vegetation Index); (**c**) NDVI (Normalized Difference Vegetation Index); (**d**) SAVI (Soil-Adjusted Vegetation Index); (**e**) ARVI (Atmospherically Resistant Vegetation Index) and (**f**) EVI (Enhanced Vegetation Index).

3.1.2. Landsat-5 TM Data

Based on the six indices derived from TM, linear models were established. The model summary and ANOVA result are shown in Table 3(b), from which it was concluded that the six indices were all extremely significant and could be used to estimate the regional LAI individually (Sig. < 0.01).

Among the six indices, it was still RVI that had the highest linear correlation with field measured LAI and simultaneously, DVI showed the least correlation. Compared to those from AVNIR-2-based indices, the linear models established using TM-based indices had lower statistical modeling accuracies, which was characterized by lower R, R^2, and higher SEE. This may be due to the effect of spatial resolution. The inconsistency between the spatial resolution (30 m) and the size of field plots (10 m) can account for the reduced accuracy.

3.1.3. MODIS NBAR Data

Due to the broad swath width of up to 2330 km for the MODIS sensor, all the field survey plots were within the MODIS coverage of one scene (h25v03). However, because of the low spatial resolution of MODIS NBAR data (500 m) and relatively close distance between some plots, sometimes two or even three field plots were within one MODIS pixel and hence only 12 groups of LAI data could be identified in the image. For those gathered in the same pixels, the average LAI value was calculated to be correlated with corresponding indices extracted from the image.

The linear correlation and modeling results are shown in Table 3(c), from which it was found that the regression models based on indices from MODIS NBAR were significant (Sig. < 0.05). *RVI* still achieved the highest linear correlation with measured and partly averaged LAI while DVI showed the least. Compared with the results from AVNIR-2 and TM, the correlations were overall much lower and the SEE were much higher. It is probably due to the reduction in the number of sample points in addition to the increase in inconsistency between the spatial resolution (500 m) and field plot size.

3.2. Multiple-Variable-Based Modeling

All of the above linear regression models are single-VI-based. However, multiple-variable-based models usually achieve a higher modeling accuracy and a lower error. The results of multiple-variable-based models using PLS regression were shown in Table 4.

The figures in this table indicated that the achieved accuracy of PLS regression model was significantly higher than those acquired from single-variable-based models. Similar as that in single-VI-based modeling, the accuracy of PLS regression model was also determined by the data

source (i.e., sensor type). When the six indices calculated from AVNIR-2 were taken as the input independent variables, the achieved R^2 was the highest while, in comparison, values from MODIS NBAR resulted in the lowest correlation between the predicted and observed parameters. It suggested that a higher spatial resolution of optical data results in a higher accuracy for LAI retrieval based on the sensor utilized here. Additionally, it should be noted that the optimal number of components, which entered the final PLS regression model, was slightly affected by the original data source.

Table 4. The result of multiple-indices-based PLS (partial least squares) regression model. The indices were derived from ALOS AVNIR-2; Landsat-5 TM; and MODIS NBAR.

Sensors	R	R^2	Optimal No. of Components	Sig.
ALOS AVNIR-2	0.968	0.937	4	0.000 **
Landsat-5 TM	0.889	0.790	3	0.000 **
MODIS NBAR	0.826	0.682	5	0.000 **

** Extremely significant correlation (Sig. $\leq$ 0.01).

3.3. Comparison of Correlation between VIs

As most vegetation indices rely on the spectral signatures of the same blue, red, and near-infrared bands of optical imagery, typically they show a strong correlation with one another. The result of PLS regression modeling reflects this autocorrelation to some extent. When building the linear models using the six indices individually, some always performed better than the others. To explore and compare the correlation among indices, the Pearson correlation was performed and the coefficients between any two of the six indices derived from ALOS AVNIR-2, Landsat-5 TM, and MODIS NBAR data were calculated. By summarizing and comparing each sensor, it was found that RVI, NDVI, and ARVI formed one group, within which, a high correlation with each other can be achieved. Similarly, the remaining three indices of DVI, SAVI, and EVI also showed a relatively high correlation with each other and hence were gathered into another group. However, when referring to their correlations with field measured LAI shown in Table 3, the two groups had completely different performance. The group consisting of RVI, NDVI, and ARVI always gave higher R^2 and lower SEE than those from DVI, SAVI, and EVI, regardless of the type of sensors. However, it should be noted that there were two years between the image and field LAI data acquisition dates which had an impact on this result.

The Pearson correlation coefficients between the same indices from different sensors were also calculated (Table 5). Results showed that the absolute values of correlation among indices were greatly affected by the sensor type. The correlation between the same indices from AVNIR-2 and TM were always significant and apparently higher than those from the other two pairs. The correlation between the same indices from AVNIR-2 and MODIS were the lowest and statistically insignificant. This indicated that the images with close spatial resolution normally resulted in higher correlations between the same indices calculated from the data. It demonstrated the importance and significance of the data source (sensor type) in remote-sensing estimation applications.

Table 5. The Pearson correlation coefficients between the same indices from different sensors: ALOS AVNIR-2 and Landsat-5 TM; Landsat-5 TM and MODIS NBAR; ALOS AVNIR-2 and MODIS NBAR; as well as ALOS AVNIR-2 and PALSAR.

Sensors	RVI/RRVI	DVI	NDVI/RNDVI	SAVI	ARVI	EVI
AVNIR-2 and TM	0.819 **	0.678 **	0.826 **	0.716 **	0.791 **	0.674 **
TM and MODIS	0.353 *	0.274	0.281	0.266	0.368 *	0.208
AVNIR-2 and MODIS	0.218	0.108	0.165	0.111	0.206	0.118
AVNIR-2 and PALSAR	0.422 *		0.335 *			

* Significant correlation (0.01 < Sig. $\leq$ 0.05); ** Extremely significant correlation (Sig. $\leq$ 0.01).

3.4. Comparison with PALSAR Indices

As PALSAR is aboard the same ALOS satellite with AVNIR-2, they have the same spatial coverage over the two forestry bureaus of Tuqiang and Amuer in the mountain area. The same 18 LAI sampling values were utilized to establish the linear regression models based on the two radar indices of RRVI and RNDVI. The modeling results are shown in Table 3(d) and Figure 6. As shown, the correlation coefficient and determination coefficient were both high (R^2 = 0.695 for RRVI and 0.694 for RNDVI). The significant probability represented the reliability of the modeling. Compared to the results from AVNIR-2-based linear regression modeling using the indices of RVI (R^2 = 0.798) and NDVI (R^2 = 0.652), no significant differences existed.

Through the Pearson correlation between the two indices, a strong collinearity was found (R = 0.998). Thus, only one variable of RRVI was included when multiple-variable stepwise regression analysis was performed. However, when correlated to the corresponding optical indices (RVI-RRVI and NDVI-RNDVI) calculated from AVNIR-2, relatively lower correlation coefficients were acquired (Table 5). It indicated that a weak collinearity existed, although there was the same spatial resolution between the data from AVNIR-2 and PALSAR sensors. The radar indices have brought in some new information, which will make a combination of the two types of data very interesting.

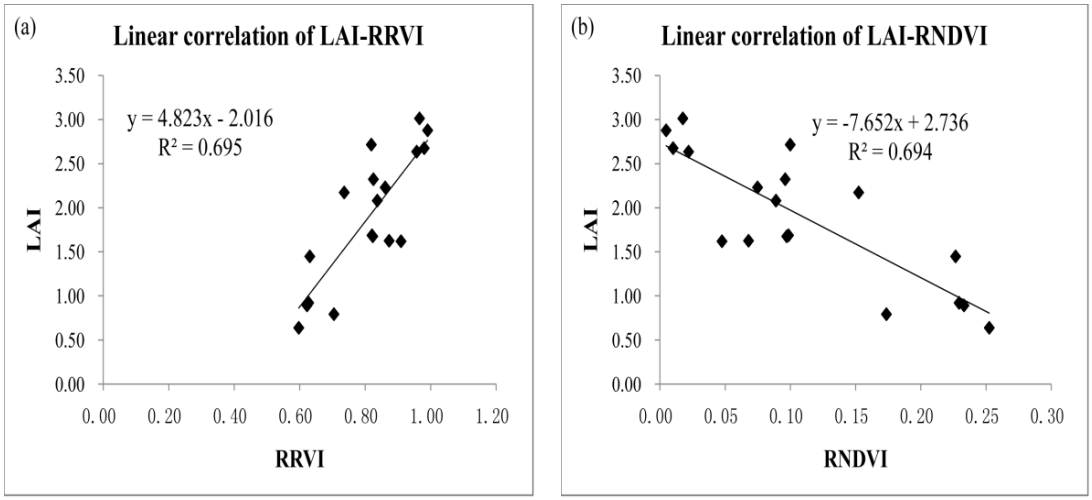

Figure 6. The linear regression models based on LAI and ALOS PALSAR-derived vegetation indices: (**a**) RRVI and (**b**) RNDVI.

4. Discussion

4.1. Sensor Features and Statistical Modeling Evaluation

In the single-variable-based regression modeling, the linear models using AVNIR-2-derived indices gave the 'best' relative performance, characterized by the highest R^2 and lowest SEE. Conversely, the correlations based on MODIS-derived indices were overall much lower and the SEE was much higher. It was probably due to the reduction of the number of sample points and the increase in inconsistency between the spatial resolution and field plot size. Normally, lower spatial resolution results in higher spatial heterogeneity within each pixel. Resampling of remote-sensing images from low to high spatial resolution has no effect on actual resolution. Thus, the inconsistency between the spatial resolution (30 m, 500 m) and the size of field plots (10 m) can account for a higher heterogeneity and reduced accuracy for TM- and MODIS-based retrieval. This was also demonstrated in some previous studies. For example, Tian et al. found that LAI retrieval errors at coarse resolution were inversely related to the proportion of the dominant land cover in such pixels. Further, large errors in LAI retrievals were incurred when forests were minority biomes in non-forest pixels compared to

when forest biomes are mixed with one another, and vice versa [31]. Fan et al. concluded that the mean values of effective LAIs retrieved from high-resolution pixels were always equal to or larger than the effective LAIs retrieved from corresponding coarse-resolution pixels [32]. All these findings were good reflections and demonstrations of scale effect in LAI studies combining remote-sensing techniques with field measurements.

In the multiple-variable-based modeling, the PLS regression algorithm was adopted. Compared to the single-variable-based modeling, a higher correlation was acquired for each sensor type, while the relative trend among sensors was maintained. The PLS regression provides the description of available data using a minimum number of adjustable components and, consequently, maximum precision and stability of regression model. In addition to the PLS regression, stepwise regression analysis was also conducted to build models using the whole collection of six indices as the input independent variables. Comparison of the stepwise regression modeling among the three optical sensors gave similar conclusions with those from PLS regression analysis. The result indicated that only partial indices entered the multiple regression models, while most were removed due to an insignificant impact or collinearity between variables. For different optical sensors, those that entered the final models all differed. For example, there were two multiple regression models produced when using the indices from ALOS AVNIR-2 as input. The RVI that showed the highest correlation with LAI entered both, while EVI was the other variable included in the second model. Comparison of the stepwise regression modeling among the three optical sensors provided a similar conclusion to that from PLS regression analysis.

4.2. Future-Oriented Points for Improvements

Although some positive results have been obtained in this scenario, there are many aspects which could be discussed and improved.

First, there were only 18 sample plots used for regression modeling because of the hot weather and difficult sampling conditions in the forests in the Greater Hinggan Mountain area. In order to expand the scope of this trial process, it is advisable to investigate more sample plots in future work for modeling and validation in larger scales.

Because of the physical mechanisms of optical and radar remote-sensing systems, the optical sensors are well suited for capturing horizontally distributed characteristics and changes represented by spectral signatures, while SAR is reasonably advantageous for the characterization of vertical features. LAI is such a basic and crucial characterization of forest attributes, both horizontally and vertically. This study revealed a satisfactory accuracy in LAI retrieval based on linear regression modeling using both optical and SAR data. Furthermore, as LAI remains consistent while the spatial scale changes, it is a crucial parameter fit for multi-scale ecological studies [33]. In this study, the linear statistical modeling method was adopted using remote sensing images with totally different spatial resolution. However, for some physically-based models, although they can be applied to scaling LAI retrievals [31], their accuracy and efficiency can be further improved. Nevertheless, it is believed that comparatively higher accuracy will be achieved when using biomass data to correlate with SAR derived variables for statistical modeling [34]. It is due to the deep penetration of microwave signals of the L-band into forest canopy and the subsequent interaction with not only leaves, but branches and trunks [35]. Compared to LAI, above-ground biomass can better characterize this complex interaction and correlate with backscatter intensity or derived indices more closely, especially for the cross-polarization as it is sensitive to volume scattering [36].

Finally, the optical image used in this study is only the multispectral data with varied spectral and spatial resolutions. The SAR data comes from the L-band PALSAR sensor alone. In future studies, other types of data can be used—including hyperspectral imagery (e.g., Hyperion) and other active remote-sensing data (e.g., LiDAR, X-band, and C-band SAR)—to explore their potential for the estimation of LAI as well as other ecological parameters. In addition, the synergic application of simultaneously combining optical images with SAR data should be considered in future studies.

5. Conclusions

In this study, the statistical modeling of data from three optical sensors of ALOS AVNIR-2, Landsat-5 TM, MODIS NBAR as well as a SAR sensor of ALOS PALSAR were evaluated and compared through statistical linear modeling with the measured LAI. Six optical vegetation indices were used for the evaluation and comparison among the three optical sensors, and simultaneously, two radar indices were calculated for the comparison between ALOS AVNIR-2 and PALSAR data. The results indicated that the higher spatial resolution of remote sensing data was, the higher the achieved accuracy in the single-variable-based modeling. The heterogeneity resulting from the gap between different remote sensing data spatial resolutions and field plot sizes contributed to the difference in the accuracy of the obtained results. Normally, during the retrieval of LAI in regional and national scales, the remote sensing data with 30 m (e.g., Landsat) was enough to provide significant results, and those with 10 m spatial resolution (e.g., ALOS AVNIR-2 and PALSAR) can bring results with higher accuracies regardless of the spectral indices used, while the MODIS cannot always meet the requirements. Considering the data acquisition costs and accuracy required, in specific applications using remote sensing techniques, the sensor types and spatial resolution should be carefully considered to achieve a cost-efficient and accurate result. The remote sensing data with a spatial resolution of not less than 30 m is always preferred at local scales.

Acknowledgments: The work in this paper was financially supported by the Natural Science Foundation of China (No. 41601368), the National Key Research and Development Program of China (No. 2016YFB0501505), the Young Talent project of the State Key Laboratory of Remote Sensing Science (No. 15RC-09), and the Japanese Government Monbukagakusho (MEXT) Scholarship (Grant No. 113378). The authors are grateful to USGS EROS, NASA LP DAAC, and JAXA EORC for providing this study with the Landsat, MODIS, ALOS AVNIR-2, and PALSAR data. Special thanks are given to Zhou Fang, Haibing Xiang and Mingren Huang, as well as the forestry technicians and workers from local forestry bureaus, for their work in the field measurements.

Author Contributions: Wei Chen is the main researcher of this work; Kazuyuki Moriya and Tetsuro Sakai commented on the statistical modeling and variable selection; Hang Yin gave great help on analyzing the results; Chunxiang Cao gave great support on field work and excellent advice on paper preparation.

Conflicts of Interest: The authors declare no conflict of interest.

References

1. Tucker, C.J.; Grant, D.M.; Dykstra, J.D. NASA's global orthorectified Landsat data set. *Photogramm. Eng. Remote Sens.* **2004**, *70*, 313–322. [CrossRef]
2. Wu, J.A.; Peng, D.L. Tree-Crown Information Extraction of Farmland Returned to Forests Using QuickBird Image Based on Object-Oriented Approach. *Spectrosc. Spectr. Anal.* **2010**, *30*, 2533–2536.
3. Bontemps, S.; Langner, A.; Defourny, P. Monitoring forest changes in Borneo on a yearly basis by an object-based change detection algorithm using SPOT-VEGETATION time series. *Int. J. Remote Sens.* **2012**, *33*, 4673–4699. [CrossRef]
4. Watanabe, M.; Shimada, M.; Rosenqvist, A.; Tadono, T.; Matsuoka, M.; Romshoo, S.A.; Ohta, K.; Furuta, R.; Nakamura, K.; Moriyama, T. Forest structure dependency of the relation between L-band sigma0 and biophysical parameters. *IEEE Trans. Geosci. Remote* **2006**, *44*, 3154–3165. [CrossRef]
5. Liang, S.L. *Quantitative Remote Sensing of Land Surfaces*; John Wiley & Sons, Inc.: Hoboken, NJ, USA, 2004; pp. 1–10.
6. Rastmanesh, F.; Moore, F.; Kharrati-Kopaei, M.; Behrouz, M. Monitoring deterioration of vegetation cover in the vicinity of smelting industry, using statistical methods and TM and ETM+ imageries, Sarcheshmeh copper complex, Central Iran. *Environ. Monit. Assess.* **2010**, *163*, 397–410. [CrossRef] [PubMed]
7. Arias, D.; Calvo-Alvarado, J.; Dohrenbusch, A. Calibration of LAI-2000 to estimate leaf area index (LAI) and assessment of its relationship with stand productivity in six native and introduced tree species in Costa Rica. *For. Ecol. Manag.* **2007**, *247*, 185–193. [CrossRef]
8. Chen, J.M.; Black, T.A. Defining leaf-area index for non-flat leaves. *Plant Cell Environ.* **1992**, *15*, 421–429. [CrossRef]

9. Chen, W.; Cao, C.X.; He, Q.S.; Guo, H.D.; Zhang, H.; Li, R.Q.; Zheng, S.; Xu, M.; Gao, M.X.; Zhao, J.; et al. Quantitative estimation of the shrub canopy LAI from atmosphere-corrected HJ-1 CCD data in Mu Us Sandland. *Sci. China Earth Sci.* **2010**, *53*, 26–33. [CrossRef]
10. Schleppi, P.; Thimonier, A.; Walthert, L. Estimating leaf area index of mature temperate forests using regressions on site and vegetation data. *For. Ecol. Manag.* **2011**, *261*, 601–610. [CrossRef]
11. Chen, W.; Moriya, K.; Sakai, T.; Koyama, L.; Cao, C.X. Post-fire forest regeneration under different restoration treatments in the Greater Hinggan Mountain area of China. *Ecol. Eng.* **2014**, *70*, 304–311. [CrossRef]
12. Guo, N. Vegetation index and its advances. *J. Arid Meteorol.* **2003**, *21*, 71–75.
13. Sharma, R.C.; Kajiwara, K.; Honda, Y. Estimation of forest canopy structural parameters using kernel-driven bi–directional reflectance model based multi-angular vegetation indices. *ISPRS J. Photogramm.* **2013**, *78*, 50–57. [CrossRef]
14. Chen, J.M.; Cihlar, J. Retrieving leaf area index of boreal conifer forests using Landsat TM images. *Remote Sens. Environ.* **1996**, *55*, 153–162. [CrossRef]
15. Chen, W.; Moriya, K.; Sakai, T.; Koyama, L.; Cao, C.X. Monitoring of post-fire forest recovery under different restoration modes based on time series Landsat data. *Eur. J. Remote Sens.* **2014**, *47*, 153–168. [CrossRef]
16. Xu, M.; Cao, C.X.; Tong, Q.X.; Li, Z.Y.; Zhang, H.; He, Q.S.; Gao, M.X.; Zhao, J.; Zheng, S.; Chen, W.; et al. Remote sensing based shrub above-ground biomass and carbon storage mapping in Mu Us desert, China. *Sci. China Technol. Sci.* **2010**, *53*, 176–183. [CrossRef]
17. Arroyo, L.A.; Johansen, K.; Armston, J.; Phinn, S. Integration of LiDAR and QuickBird imagery for mapping riparian biophysical parameters and land cover types in Australian tropical savannas. *For. Ecol. Manag.* **2010**, *259*, 598–606. [CrossRef]
18. Andersen, H.E.; Strunk, J.; Temesgen, H.; Atwood, D.; Winterberger, K. Using multilevel remote sensing and ground data to estimate forest biomass resources in remote regions: A case study in the boreal forests of interior Alaska. *Can. J. Remote Sens.* **2011**, *37*, 596–611. [CrossRef]
19. Chen, X.; Vierling, L.; Deering, D.; Conley, A. Monitoring boreal forest leaf area index across a Siberian burn chronosequence: A MODIS validation study. *Int. J. Remote Sens.* **2005**, *26*, 5433–5451. [CrossRef]
20. Chowdhury, T.A.; Thiel, C.; Schmullius, C.; Stelmaszczuk-Gorska, M. Polarimetric Parameters for Growing Stock Volume Estimation Using ALOS PALSAR L-Band Data over Siberian Forests. *Remote Sens.* **2013**, *5*, 5725–5756. [CrossRef]
21. Han, N.; Du, H.Q.; Zhou, G.M.; Xu, X.J.; Cui, R.R.; Gu, C.Y. Spatiotemporal heterogeneity of Moso bamboo aboveground carbon storage with Landsat Thematic Mapper images: A case study from Anji County, China. *Int. J. Remote Sens.* **2013**, *34*, 4917–4932. [CrossRef]
22. Schroeder, T.A.; Wulder, M.A.; Healey, S.P.; Moisen, G.G. Detecting post-fire salvage logging from Landsat change maps and national fire survey data. *Remote Sens. Environ.* **2012**, *122*, 166–174. [CrossRef]
23. Millin-Chalabi, G.; McMorrow, J.; Agnew, C. Detecting a moorland wildfire scar in the Peak District, UK, using synthetic aperture radar from ERS-2 and Envisat ASAR. *Int. J. Remote Sens.* **2014**, *35*, 54–69. [CrossRef]
24. Pearson, R.L.; Miller, L.D. Remote Mapping of Standing Crop Biomass for Estimation of the Productivity of the Shortgrass Prairie. In Proceedings of the Eighth International Symposium on Remote Sensing of Environment, Ann Arbor, MI, USA, 2–6 October 1972; Willow Run Laboratories, Environmental Research Institute of Michigan: Ypsilanti, Michigan, 1972; pp. 1355–1381.
25. Jordan, C.F. Derivation of leaf area index from quality of light on the forest floor. *Ecology* **1969**, *50*, 663–666. [CrossRef]
26. Rouse, J.W.; Haas, R.H.; Schell, J.A.; Deering, D.W. Monitoring Vegetation Systems in the Great Plains with ERTS. In Proceedings of the Third Earth Resources Technology Satellite-1 Symposium, Washington, DC, USA, 10–14 December 1973; NASA/GSFC: Greenbelt, MD, USA, 1974; pp. 309–317.
27. Huete, A.R. A soil-adjusted vegetation index (SAVI). *Remote Sens. Environ.* **1988**, *25*, 295–309. [CrossRef]
28. Kaufman, Y.J.; Tanre, D. Atmospherically resistant vegetation index (ARVI) for EOS-MODIS. *IEEE Trans. Geosci. Remote* **1992**, *30*, 261–270. [CrossRef]
29. Liu, H.Q.; Huete, A.R. A feedback based modification of the NDVI to minimize canopy background and atmosphere noise. *IEEE Trans. Geosci. Remote* **1995**, *33*, 457–465.
30. Haenlein, M.; Kaplan, A.M. A Beginner's Guide to Partial Least Squares Analysis. *Underst. Stat.* **2004**, *3*, 283–297. [CrossRef]

31. Tian, Y.H.; Wang, Y.J.; Zhang, Y.; Knyazikhin, Y.; Bogaert, J.; Myneni, R.B. Radiative transfer based scaling of LAI retrievals from reflectance data of different resolutions. *Remote Sens. Environ.* **2003**, *84*, 143–159. [CrossRef]
32. Fan, W.J.; Gai, Y.Y.; Xu, X.R.; Yan, B.Y. The spatial scaling effect of the discrete-canopy effective leaf area index retrieved by remote sensing. *Sci. China Earth Sci.* **2013**, *56*, 1548–1554. [CrossRef]
33. Zheng, G.; Moskal, L.M. Retrieving Leaf Area Index (LAI) Using Remote Sensing: Theories, Methods and Sensors. *Sensors* **2009**, *9*, 2719–2745. [CrossRef] [PubMed]
34. Mitchard, E.T.A.; Saatchi, S.S.; Woodhouse, I.H.; Nangendo, G.; Ribeiro, N.S.; Williams, M.; Ryan, C.M.; Lewis, S.L.; Feldpausch, T.R.; Meir, P. Using satellite radar backscatter to predict above-ground woody biomass: A consistent relationship across four different African landscapes. *Geophys. Res. Lett.* **2009**, *36*, L23401. [CrossRef]
35. Kobayashi, S.; Widyorini, R.; Kawai, S.; Omura, Y.; Sanga-Ngoie, K.; Supriadi, B. Backscattering characteristics of L-band polarimetric and optical satellite imagery over planted acacia forests in Sumatra, Indonesia. *J. Appl. Remote Sens.* **2012**, *6*, 063525.
36. Suzuki, R.; Kim, Y.; Ishii, R. Sensitivity of the backscatter intensity of ALOS/PALSAR to the above-ground biomass and other biophysical parameters of boreal forest in Alaska. *Polar Sci.* **2013**, *7*, 100–112. [CrossRef]